



PCCP

**Theoretical and experimental study on the  $O(^3P) + 2,5$ -  
dimethylfuran reaction in the gas phase**

Journal:	<i>Physical Chemistry Chemical Physics</i>
Manuscript ID	CP-ART-04-2021-001724.R1
Article Type:	Paper
Date Submitted by the Author:	24-Jun-2021
Complete List of Authors:	Giustini, Andrea; University of L'Aquila Department of Physical and Chemical Sciences Aschi, Massimiliano; University of L'Aquila Department of Physical and Chemical Sciences Park, Heejune; University of San Francisco College of Arts and Sciences, Chemistry Meloni, Giovanni; University of San Francisco College of Arts and Sciences, Department of Chemistry

SCHOLARONE™  
Manuscripts

Cite this: DOI: 00.0000/xxxxxxxxxx

# Theoretical and experimental study on the $O(^3P) + 2,5$ -dimethylfuran reaction in the gas phase

Andrea Giustini,<sup>a</sup> Massimiliano Aschi,<sup>a\*</sup> Heejune Park,<sup>b</sup> and Giovanni Meloni<sup>ab\*</sup>

Received Date

Accepted Date

DOI: 00.0000/xxxxxxxxxx

In this work we report a joint experimental and computational study on the 2,5-dimethylfuran oxidation reaction in the gas-phase initiated by atomic oxygen  $O(^3P)$ . The experiments have been performed by using a vacuum-ultraviolet synchrotron radiation at the Advanced Light Source (ALS) of the Lawrence Berkeley National Laboratory (LBNL), at the temperature of 550 K and the pressure of 8 Torr. The experimental data were supported by quantum-chemical calculations along with a kinetic model, also taking into account possible involvement of different magnetic states, performed in the framework of the RRKM theory. Propyne, acetaldehyde, methylglyoxal, dimethylglyoxal, 3-penten-2-one, 2,5-dimethylfuran-3(2H)-one, and 1,2-diacetyl ethylene have been identified as the main primary products arising in the conditions of the experiment. Our computational model suggests that these species can be formed at the concentration and branching ratio experimentally observed only in the presence of non-negligible fraction of non-thermalized intermediates.

## 1 Introduction

Energy allows us to access convenient lifestyles. Owing to this provision of energy and the human population growth, the global demand for energy, which mostly relies on fossil fuels, is increasing rapidly. More than 80% of this requirement has been fulfilling through fossil fuels, a limited depleting resource.<sup>1,2</sup> To reduce the usage of fossil fuels and meet the demand, diverse resources are being studied and biofuels have been receiving great attention.<sup>3-9</sup> Among the many candidates of biofuel, 2,5-dimethylfuran (hereafter: 2,5-DMF) has attracted many researchers to investigate its properties.<sup>8-13</sup> 2,5-DMF has a high volumetric energy density (31.5 MJ/L), in comparison gasoline has a value of 32.2 MJ/L, with a high octane number (119).<sup>11</sup> Higher octane numbers tend to reduce knocking in an engine and thus increase fuel efficiency and lessen damages to the engine.<sup>11-14</sup> Due to its great potential as an alternative fuel, many studies regarding production and combustion have been carried out. In 2007, Román-Leshkov and co-workers<sup>14</sup> proposed a two step synthesis of 2,5-DMF. They successfully achieved great yield in liquid-phase hydrolysis (71%) and vapor-phase hydrogenolysis (76-79%). This discovery motivated other scientists to explore alternative produc-

tion mechanisms of 2,5-DMF.<sup>10,15-17</sup> Binder and Raines<sup>10</sup> proposed synthesis of hydroxymethylfurfural (HMF) from lignocellulosic biomass, abundant raw material, which opened up new possibilities for 2,5-DMF as a commercial fuel. Chidambaram and Bell<sup>17</sup> successfully converted glucose to 2,5-DMF. They utilized ionic liquids and acetonitrile as a cosolvent for dehydration of glucose to HMF and reported great yield. Fructose, isomerized form of glucose, was also studied and achieved over 95% yield of 2,5-DMF through heating a solution of HMF in refluxing tetrahydrofuran (THF) with formic acid, sulfuric acid, and Pd/C (carbon-supported palladium) by Thananathanachon and Rauchfuss.<sup>16</sup> Along with various synthetic methodologies, 2,5-DMF performance has been investigated extensively.<sup>11 18-24</sup> Zhong and co-workers<sup>11</sup> carried out experiments employing a single-cylinder gasoline direct-injection (GDI) research engine and reported physicochemical similarity of combustion and emission between 2,5-DMF and gasoline. Zhang and co-workers<sup>19</sup> found that the mixture of 2,5-DMF (40% by volume fraction) and diesel, referred as D40, reduces soot emissions dramatically compared with basic diesel when they go through combustion in a single cylinder diesel engine. They also performed an experiment with 2-ethylhexyl nitrate added into the D40 and observed a further reduction of soot emissions.<sup>20</sup> However, 2,5-DMF is seen to be the least promising among the furanic biofuels,<sup>25</sup> with 2-MF showing a better behavior in terms of performance and harmful emissions.<sup>26</sup> Tran et al.<sup>27</sup> nicely summarized the kinetics mechanisms and reaction classes relevant to biofuel oxidation. They also stated that radical addition reactions to the double bond of furans and furan derivatives have been poorly investigated, thus

<sup>a</sup> Dipartimento di Scienze Fisiche e Chimiche, Università degli Studi dell'Aquila, Via Vetoio, 67100 L'Aquila, Italy

<sup>b</sup> Department of Chemistry, University of San Francisco, 2130 Fulton St, San Francisco, 94117 California, United States.

\* Corresponding Authors; E-mail: massimiliano.aschi@univaq.it; gmeloni@usfca.edu

† Electronic Supplementary Information (ESI) available: [details of any supplementary information available should be included here]. See DOI: 10.1039/cXCP00000x/

pointing out the significance of the present study to provide new details about elementary reactions initiated by radicals. Among the studies associated with the combustion research field, Grela et al.<sup>28</sup> studied the pyrolysis of 2,5-DMF spanning the temperature range from 1050 to 1270 K under very low pressure conditions (1 mTorr). They detected H<sub>2</sub>O, CO, C<sub>6</sub>H<sub>6</sub> and C<sub>5</sub>H<sub>8</sub> and proposed two reaction mechanisms to explain the formation of these products. The 2,5-DMF thermal decomposition was also studied by Lifshitz et al.<sup>29</sup> behind reflected shock waves at a similar temperature range under 2-3 atm. They analyzed the products via gas-chromatography, quantified the species and proposed the decomposition of 2,5-DMF to be initiated by a 1,2-methyl migration followed by ring opening to give biradical intermediates undergoing CO-elimination to produce various C<sub>5</sub>H<sub>8</sub> isomers as reported by Grela et al.<sup>28</sup> To analyze mole fractions of intermediates and products from combustion of 2,5-DMF/oxygen/argon mixture, synchrotron vacuum ultraviolet photoionization mass spectrometry was utilized by Liu et al.<sup>21</sup> Their instrument consists of a low-pressure combustion system in which reactants are mixed and subsequently flowed into a burner to ignite the mixture and analyze the arising flame species afterwards. At the pressure of 30 Torr, they calculated mole fractions profiles of the major products and the intermediates, such as 2-(5-methyl)furylmethyl radical, 2,5-dimethylene-2,5-dihydrofuran, 1-oxo-1,3,4-pentatriene, 2-furylmethyl radical, fulvene, and cyclopentadienyl radical, as a function of their distance from the burner by developing a kinetic model from Somers et al.<sup>30</sup> where 2872 reactions involving 565 species are included with each corresponding temperature- and pressure-dependent rate constants. Reactions between radicals and 2,5-DMF have been investigated as well. Wei et al.<sup>22</sup> studied primary chemistry products arising from combustion of 2,5-DMF/oxygen/argon mixture at 30 Torr via mass spectrometry. The detected intermediates were ionized through the tunable synchrotron radiation and identified based on the match between the experimental onsets of the corresponding recorded photoionization curves (PI) and the G3B3-level calculated adiabatic ionization energies (AIE) as well as simulated and tabulated PI curves. H-abstraction, H-addition and OH-addition products were identified, including 5-methylfurfural, (Z)-1-oxo-1,3,4-pentatriene, 2-ethyl-5-methylfuran, 2-methylfuran, (2Z,3E)-1-oxo-1,3-pentadiene and 2-oxo-2,3-dihydro-5-methylfuran. The OH radical-initiated reaction of 2,5-DMF was analyzed by Aschmann et al.<sup>23</sup> identifying (E, Z)-3-hexene-2,5-dione as the main products. In our previous study, focused on the methylidyne radical (CH and CD) reaction with 2,5-DMF, two main pathways were found: CH addition and insertion.<sup>24</sup> Theoretical studies explore the unimolecular decomposition pathways of 2,5-DMF including C–H bond fission of the side chain methyl groups, ring opening, and  $\alpha$ -,  $\beta$ -carbenes formation via H-atom and CH<sub>3</sub>-group migration.<sup>31,32</sup> Based on the energetics and the kinetics, these studies show that at very high temperatures the most dominant channel is the 3,2-H shift leading to hexa-3,4-dien-2-one via  $\beta$ -carbene intermediate. C–H bond fission is also found to be occurring as a minor channel, whereas the methyl group migration is found to be uncompetitive with the other channels up to 2000 K. The kinetic study of the reaction of atomic oxygen (O(<sup>3</sup>P))

with furan, 2-methylfuran (2-MF), and 2,5-DMF was performed by Yoshizawa and co-workers.<sup>33</sup> By following the O(<sup>3</sup>P) concentration up to 600  $\mu$ s at temperature of around 1150 K and a pressure of almost 1 Pa, they found that O(<sup>3</sup>P)-depletion rate become faster as methyl groups increase.

Over the last decades, reactions of O(<sup>3</sup>P) with unsaturated hydrocarbons have been investigated due to their importance as one of the fundamental oxidation routes in combustion science.<sup>34–38</sup> Many studies, both theoretical and experimental, highlighted this route as a significant loss channel responsible for unimolecular and chain-propagating reactions leading to products. For instance, Miller et al.<sup>39</sup> found the reaction with O(<sup>3</sup>P) to be the dominant removal step under a wide range of temperature accounting for up to 70% of the overall product yield. On the other hand, O(<sup>3</sup>P) + short-chain hydrocarbons reaction, such as propene and ethylene, have also been studied to accomplish a fully detailed understanding of all the possible consumption mechanisms involving these species.<sup>34–37</sup> In this work, with the aim to assess the first steps of radical-initiated reactions, specifically with O(<sup>3</sup>P), both relevant to the chemistry of the atmosphere and combustion, the oxidation of 2,5-DMF initiated by O(<sup>3</sup>P) was investigated at 550 K and 8 Torr of pressure (He as bath gas) through synchrotron radiation coupled with multiplexed photoionization mass spectrometry (MPIMS) at the Lawrence Berkeley National Laboratory (LBNL). The products were then identified by measuring their photoionization (PI) spectra and rationalized through a computational procedure. In this respect, we first carried out quantum-chemical calculations for identifying the critical points on the singlet and triplet surfaces, as well as the possible channels for the interconversion from one magnetic surface to the other. Subsequently, a kinetic model was constructed in the framework of the Rice-Ramsperger-Kassel-Marcus Transition State Theory<sup>40,41</sup> (RRKM-TST), including its non-adiabatic version<sup>42,43</sup>, and solved using a 1-dimensional (1-D) Master Equation. Given the number of utilized approximations, it is important to remark that the main aim of our calculations is to provide a semi-quantitative rationale of the species experimentally observed in the millisecond time-domain.

## 2 Experimental Methods

The Chemical Dynamics Beamline 9.0.2 at the Advanced Light Source (ALS) of the Lawrence Berkeley National Laboratory was utilized to carry out this experiment.<sup>44</sup> Reaction species were identified through multiplexed time- and energy-resolved mass spectrometry coupled with tunable synchrotron radiation for photoionization. Further details of the experimental set up are discussed in previous publications.<sup>45–48</sup> 2,5-DMF (Sigma-Aldrich, purity  $\geq$  99%) was further purified through the freeze-pump-thaw technique. The vapor from purified 2,5-DMF was collected into a gas cylinder and diluted to roughly 0.54% (20.35 Torr of 2,5-DMF in 3739 Torr total with He). A 4 Hz pulsed unfocused 351 nm XeF excimer laser initiated the reaction by photolyzing the radical precursor NO<sub>2</sub>, which produced O(<sup>3</sup>P). The photolytic precursor, NO<sub>2</sub>, and 2,5-DMF were introduced in the slow-flow reactor (62 cm long and 1.05 cm of inner diameter) together with He using calibrated mass flow controllers. The

concentration of  $\text{NO}_2$  used in this experiment is calculated to be  $2.67 \times 10^{14}$  molecule  $\text{cm}^{-3}$  at 550 K. Based on the reported quantum yield of 1.00 for  $\text{O}(^3\text{P})$  at 351 nm<sup>49</sup> and the absorption cross section of  $4.62 \times 10^{-19}$   $\text{cm}^2$ ,<sup>50</sup>  $\text{O}(^3\text{P})$  concentration is calculated to be  $6.33 \times 10^{12}$  molecule  $\text{cm}^{-3}$  at 550 K. The concentrations of 2,5-DMF, calculated based on flow, temperature, pressure, and sample purity is  $7.64 \times 10^{12}$  molecule  $\text{cm}^{-3}$  at 550 K. Reaction species went through a 650  $\mu\text{m}$  diameter pinhole into an ionization region, where the synchrotron radiation crossed and ionized the species if their ionization energies are equal or lower than the tuned synchrotron radiation energy. The ions were then collimated, focused, accelerated by 50 kHz pulses and detected through orthogonal-acceleration time-of-flight mass spectrometry. The pressure inside the reactor was kept constant (8 Torr) by gas removal using a closed-loop feedback throttle valve and through a capacitive manometer. The reactor temperature was adjusted using 18  $\mu\text{m}$  thick resistive nichrome heating tape wrapped around the reactor tube. Insulation for thermal homogeneity of the tube was achieved by a layer of square-weave, yttria-stabilized zirconia cloth. The collected data consisted of the ion signal as a function of photon energy (eV), reaction time (ms), and mass-to-charge ratio (m/z), which formed a three-dimensional data block. The prephotolysis signal was removed through background subtraction and the energy-dependent signal was normalized against the photocurrent measured by a calibrated photodiode. Two-dimensional slices of the three-dimensional data were obtained by fixing one variable. The reactants show negative ion signal (depleting species) from kinetic time plots (ion signal vs kinetic time), whereas products have a positive signal. The signal was integrated in the time range 0-50 ms to minimize the presence of secondary product signal. The photoionization (PI) spectra were collected in the energy range of 7.9-11.0 eV with 25 meV step size (200 shots/step and averaged). The collected PI spectra were used for products identification by comparing the measured spectra with literature or simulated PI curves based on the Franck-Condon (FC) principle. Due to the complexity in detecting and analyzing various isomer species, the photon energy step size, and the energy resolution, an uncertainty of  $\pm 0.05$  eV is given for the measured ionization energies of species with a spectral onset.

### 3 Computational Methods

#### 3.1 Quantum Chemical Calculations

Quantum chemical calculations were carried out using two different methods: (i) CBS-QB3 composite method<sup>51,52</sup> and, when required by the length or complexity of the calculation, (ii) Density Functional Theory with the wB97XD functional<sup>53</sup> and the 6-311+G(2d,p) basis set (hereafter we refer to this level of theory simply with the acronym DFT). Critical points on the 2,5-DMF/ $\text{O}(^3\text{P})$  surface were located and characterized as true minima and first order saddle points, i.e., Transition Structures (TS) by calculating the corresponding harmonic vibrational frequencies. For these calculations, the CBS-QB3 method was used as implemented in the GAUSSIAN09<sup>54</sup> package. Adiabatic ionization energies (AIE), reaction energies and enthalpies were then eval-

uated with the same composite method with a reported mean average deviation of 4-5 kJ/mol.<sup>51,52</sup> Adiabatic ionization energies, used for simulating photoelectron spectra (PE), were calculated by subtracting the zero-point vibrational corrected energy ( $E_0$ ) of the optimized neutral from the  $E_0$  of the optimized cation. The identification of the products was accomplished by comparing experimental PI spectra from this study with literature PI spectra. When literature PI spectra were not available, Franck-Condon (FC)<sup>55-58</sup> and Frank-Condon-Herzberg-Teller (FCHT)<sup>55</sup> simulations were performed to obtain simulated PE spectra by approximating the Frank-Condon factors based on the vibronic transitions from the neutral to the cation. The actual mechanical role of each of the located TS was then ascertained through Intrinsic Reaction Coordinate (IRC) calculations<sup>59,60</sup>. Possible involvement of intersystem crossing (ISC), i.e., mutual hop from one magnetic surface to the other,<sup>61</sup> was also taken into account by adopting an approximate approach, which assumes that the system can cross in the proximity of the Minimum Energy Crossing Point (MECP). This latter point is represented by the minimum of the crossing hyperseam, i.e., intersection between multidimensional hypersurfaces,<sup>62</sup> and, hence, it can be considered as the actual TS for processes involving ISC.<sup>63</sup> For MECPs identification we employed a standard analytical-gradient-based approach<sup>62,63</sup> with the DFT method with the GAMESS US software.<sup>64</sup> Geometrical details of all the critical points and MECPs are reported in the Supplementary Information (S.I.).

#### 3.2 Kinetic Model

The main goal of this part of the study is to test the validity of the mechanistic picture emerged by the Quantum Chemical calculations focusing, in particular, on the interpretation of the experimentally detected products. For this purpose we solved the 1-dimensional (1-D) Master Equation, neglecting the effect of angular momentum conservation and, hence, well aware of the consequent limitations of the model. This was accomplished through the MultiWell program package provided by Barker and co-workers,<sup>65,66</sup> assuming the validity context of the RRKM theory used for calculating all the microcanonical rate coefficients. The latter were evaluated on the basis of the harmonic frequencies and the geometries of all the critical points, using the DenSum and Ktools softwares implemented in the MultiWell packages<sup>65</sup> for tight and loose TS, respectively. In particular, for the loose transition states leading to the formation of oxygen addition to DMF (see intermediates C and D in the Results section) we performed constrained optimizations, i.e., at fixed DMF-oxygen distances, followed by the estimation of the harmonic vibrational frequencies orthogonal to the path. These calculations were carried out at the DFT level of theory and the details of these structures are reported in the S.I. In the case of ISC channels, including the MECPs kinetically treated as tight TSs, we adopted a slightly different procedure as reported in the next subsection. The contribution of tunnelling was taken into account by utilizing the Eckart potential function<sup>67</sup> for those reactions involving an hydrogen transfer. All the simulations, propagated up to  $10^{-2}$  seconds were initiated by a chemically activated encounter complex formed as

low as the reactants at the temperature of the experiment. Helium was used as bath gas and, for this purpose, bimolecular deactivation was modelled using a biexponential down model with a temperature dependent energy transfer ( $\Delta E_{\text{down}}$ ) provided by Nguyen et al.<sup>68</sup> and Weston et al.<sup>69</sup> The Lennard-Jones parameters for He and all the involved intermediates were taken from Hippler et al.<sup>70</sup> and adapted from chemically similar species<sup>65</sup>. We did not carry out further evaluation of the reliability of these parameters in the present study. All the reaction channels, excluding the ones leading to bond cleavages, were treated as reversible steps in the kinetic model.

### 3.3 Rate coefficients for non-adiabatic reactions

To estimate the relevant microcanonical rate coefficients for reactions involving ISC we employed an RRKM-like approach<sup>42,43</sup> making use of the following equation:

$$k(E) = \frac{2}{h\rho(E)} \int_0^E \rho^{MECP}(E - E_h) P_{sh}(E_h) dE_h \quad (1)$$

where  $h$  is the Planck constant,  $\rho^{MECP}(E - E_h)$  corresponds to the density of the rovibrational states at the MECP evaluated also in this case using DenSum software.<sup>65</sup> We utilized the eigenvalues of the MECP effective Hessian matrix as described in Bo Yang et al.<sup>71</sup> Finally, the term  $P_{sh}$ , which provides us with the hopping probability at the crossing, was estimated at the MECP using the Landau-Zeener formula:

$$\rho^{MECP}(E - E_h) = \frac{2\pi V_{12}^2}{h\Delta F} \sqrt{\frac{\mu_h}{2(E - E_{MECP})}} \quad (2)$$

In this expression, the term  $E - E_{MECP}$  is the energy available along the semi-classical reaction coordinate,  $\mu_h$  is the corresponding reduced mass,  $V_{12}$  is the norm of the the spin-orbit coupling (average of the interactions between the singlet and all the triplet substates) estimated at the same level of theory (DFT) within the Linear Response Theory using the DALTON software<sup>72</sup>. Finally,  $\Delta F$  is the norm of the gradient difference between the two crossing surfaces.

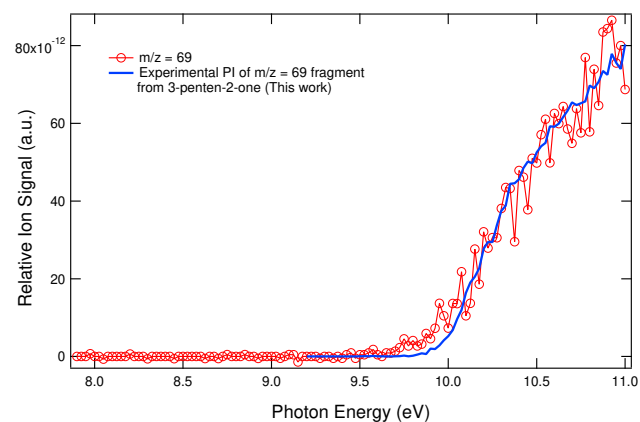
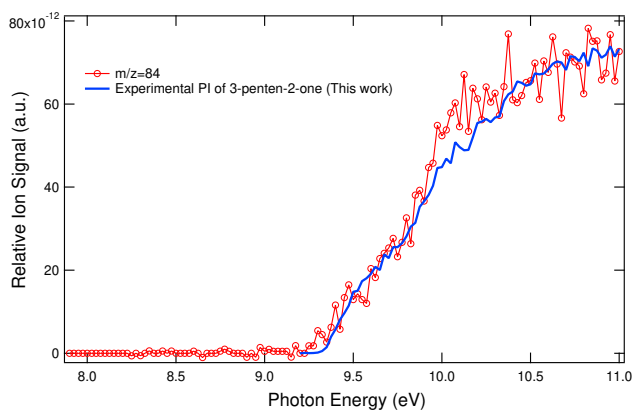
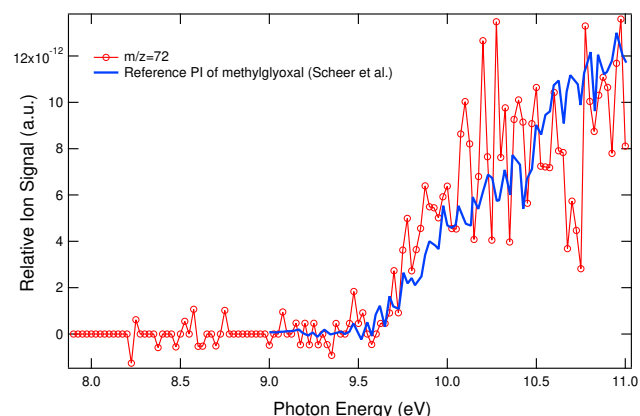
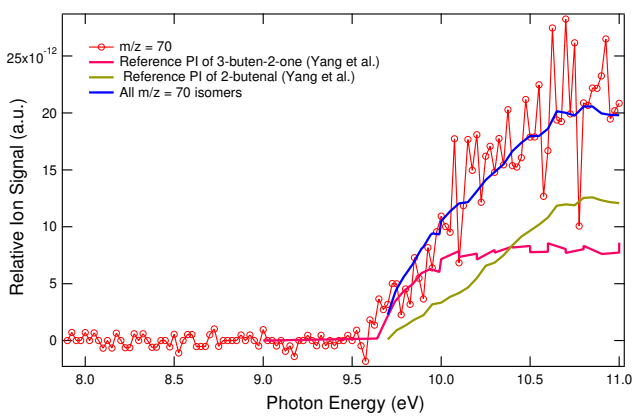
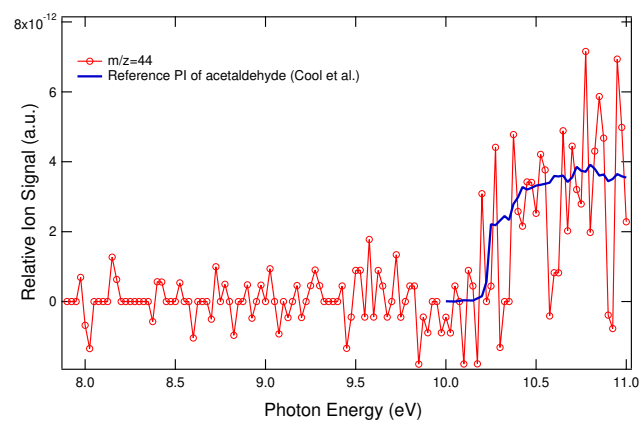
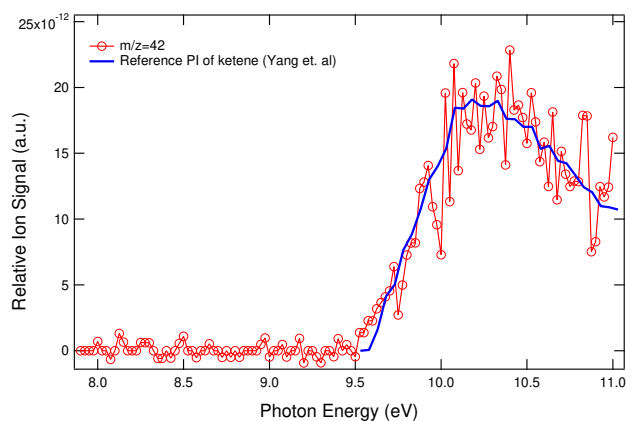
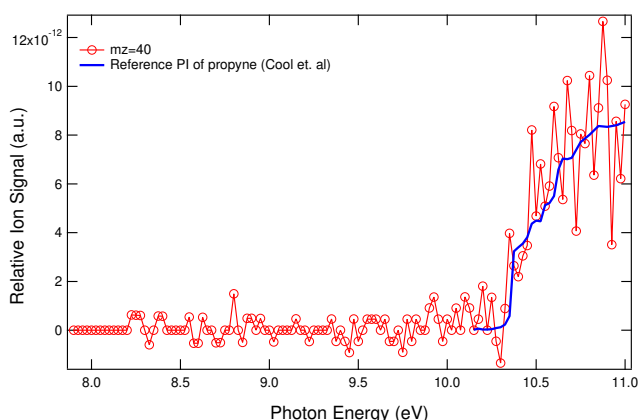
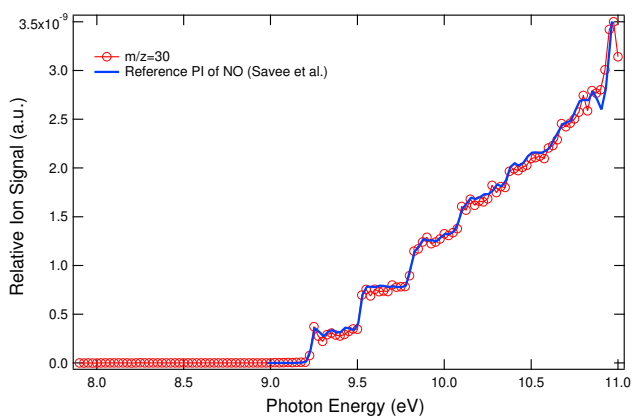
## 4 Results and Discussions

### 4.1 Experimental section

Figure 1 depicts all the experimental PI spectra along with either the literature or simulated PI. Figure 1(a) shows the literature PI spectrum of nitrogen oxide  $\text{NO}$ <sup>36</sup> superimposed onto the experimental PI plot of  $m/z = 30$ . Nitrogen oxide arises from the  $\text{NO}_2$  photolysis process. Figure 1(b) refers to the  $m/z = 40$  experimental PI plot, which matches very well the literature PI spectrum of propyne<sup>73</sup>. Its isomer allene is not observed because there is no signal detected at its AIE of 9.7 eV.<sup>74</sup>

Figure 1(c) illustrates the literature PI spectrum of ketene<sup>75</sup> superimposed onto the experimental PI plot of  $m/z = 42$ . Figure 1(d) depicts the  $m/z = 44$  experimental PI spectrum, which has been found to be consistent with the literature acetaldehyde PI spectrum.<sup>74</sup> Ethanol is not observed because no signal is detected at its AIE of 9.33 eV,<sup>76</sup> much lower than acetaldehyde AIE. Figure 1(e) refers to the  $m/z = 70$  experimental PI plot. The very

first part of this PI spectrum matches the reference PI curve of 3-buten-2-one up to 9.9 eV and then starts deviating. This can be ascribed to the presence of 2-butenal isomer, with an onset at 9.7 eV. To the best of our efforts, no unimolecular pathways have been found to give an explanation for 2-butenal formation, therefore, it may derive from a secondary chemistry mechanism. On the basis of CBS-QB3 calculations, we can also assign this mass to the dissociative photoionization fragment of diacetyl ethylene, which can undergo a fast McLafferty rearrangement upon ionization yielding a  $m/z = 70$  daughter ion and neutral  $m/z = 42$ . The experimental onset of  $9.60 \pm 0.05$  eV is in good agreement with the CBS calculated appearance energy (AE) of roughly  $9.70 \pm 0.05$  eV, backing up our assumption and making this assignment ambiguous. Figure 1(f) shows then literature PI spectrum of methylglyoxal<sup>77</sup> superimposed onto the experimental PI plot of  $m/z = 72$ . Despite the good agreement with the experimental PI spectrum onset, the second part of the curve at higher photon energies is very noisy due to the poor signal-to-noise ratio, hence leading to a greater error for the assignment. Based on our mass resolution,  $m/z = 72$  is observed at 72.031 a.m.u. very close to the methylglyoxal mass of 72.021 a.m.u., therefore, we can exclude the presence of 2-butanone ( $\text{C}_4\text{H}_8\text{O}$ ) with a mass of 72.057 a.m.u. Figures 1(g) and 1(h) present the PI spectrum of 3-penten-2-one and one of its photodissociation ionization fragment, superimposed onto the experimental PI spectra of  $m/z = 84$  and 69, respectively. Figure 1(i) illustrates the PI spectrum integrated from the literature photoelectron spectrum of dimethylglyoxal<sup>78</sup> in the 8-11 eV energy range, superimposed onto the experimental PI plot of  $m/z = 86$ . The first part of the experimental spectrum is perfectly reproduced up to 10 eV, from which it starts deviating. At higher photon energy the experimental signal starts deviating from the literature spectrum. This might be due to a secondary chemistry product or a dissociative photoionization fragment of a larger mass. Finally, figure 1(j) shows the simulated PI spectra of 1,2-diacetyl ethylene and 2,5-dimethylfuran-3(2H)-one summed up to match the experimental  $m/z = 112$  PI spectrum. The CBS-QB3 calculated AIE are  $9.46 \pm 0.05$  eV and  $9.01 \pm 0.05$  eV for 1,2-diacetyl ethylene and 2,5-dimethylfuran-3(2H)-one, respectively. We did not report products from thermal decomposition as we expected based on the experimental temperatures in agreement with the Yoshizawa and co-workers<sup>33</sup> findings, where less than 10% of reactants decay is due to thermal decomposition at much higher temperatures (around 1150 K). Although the Liu et al.<sup>21</sup> experiment was conducted in totally different conditions in terms of pressure, temperature and reactants involved (DMF/ $\text{O}_2$  lean and rich mixture), we point out, among the several products measured in their experiment, short-chain products formation, such as propyne, ketene, and acetaldehyde similarly with our experiment, whereas no matches can be found regarding the other reaction species. No similarities in the identified oxidation products are reported between our experiment and the Wei et al.<sup>22</sup> experiment as well.



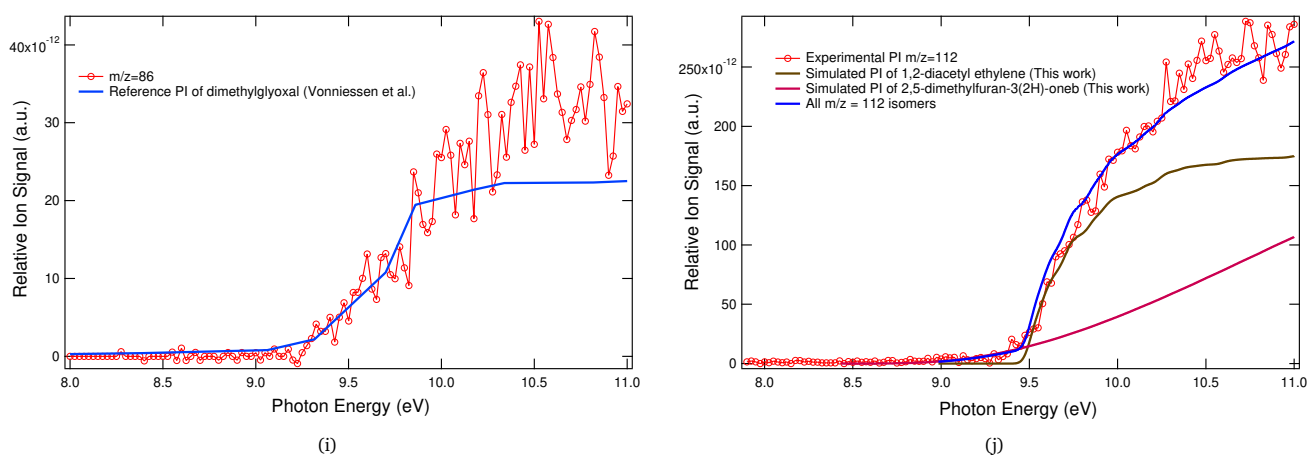


Fig. 1 Experimental photoionization spectra measured in the MPIMS experiment at 550 K with literature and simulated PI spectra superimposition.

## 4.2 Computational Section

Generally, atmospheric oxidations involving volatile organic compounds (VOCs) need radicals like hydroxyl (OH) and atomic oxygen  $O(^3P)$ , as well as nitrogen oxides ( $NxOy$ ), to be initiated. Previous studies suggest that in the case of  $O(^3P)$  initiated reactions for unsaturated carbon molecules two main pathways can be expected: (1) oxygen atom addition to the unsaturated bonds<sup>34–38</sup> and (2) hydrogen abstraction.<sup>79,80</sup> Figure 2 presents the CBS-QB3 relative energies of these two pathways, which are in good agreement with the Yoshizawa and co-workers<sup>33</sup> study, although they present the early steps of the reaction solely occurring on the triplet surface, stating that it is sufficient to account for primary chemistry pathways, which, in the light of our findings, appears to be a poor description of the overall potential energy surface and dynamics. The B radical formation is a strongly endothermic channel owing to the large strength of the ring C-H bonds. On the other hand, H-abstraction from methyl groups leading to the radical A appears as energetically more feasible. However, additional calculations (not reported) have indeed showed that this channel eventually leads to 5-methylfurfuryl alcohol whose AIE of 8.02 eV, evaluated using the CBS-QB3 composite method, makes this species as completely inconsistent with the measured experimental onset of the corresponding detected  $m/z = 112$  PI spectrum from the MPIMS experiment. Moreover, a relatively high electronic energy barrier of 16 kJ/mol, estimated at DFT level of theory for such H-abstraction channel (see S.I. for additional details), makes such a route as hardly competitive, with respect to the barrierless (see also S.I.) addition routes leading to C and D intermediates. These findings are in good agreement with Yoshizawa and co-workers<sup>33</sup> where a CBS-QB3 activation energy of roughly 20 kJ/mol is reported for what concerns the H-abstraction channel, whereas addition channels are reported barrierless for adduct D formation and with an unquantified tiny barrier for adduct C formation. At the investigated temperature, a sizeable free energy barrier of 55 kJ/mol has been found for the H-abstraction route, whereas free energy barriers of 37 kJ/mol and 32 kJ/mol have been calculated for adduct C and D forma-

tion, respectively. As the H-abstraction route is characterized by an actual saddle point with a pure electronic energy barrier (16 kJ/mol), the  $O(^3P)$  addition routes barriers are solely ascribable to entropic effects whose contribution is included by evaluating the molecular partition function at 550 K. In light of these findings, also consistent with previous investigations<sup>35–38,80–82</sup>, we limited our attention to the  $O(^3P)$  addition routes appearing to be the most viable ones to account for the products resulting from primary-chemistry reactions.

The potential energy diagram is reported in Figure 3. The reaction is, therefore, assumed to start on the triplet surface with the formation of the intermediates C and D, which, at least in principle, can either adiabatically evolve on the triplet surface or undergo a spin transition through intersystem crossing. However, concerning the species C we couldn't locate any low-energy triplet reaction route and, hence, this species is expected to cross to the singlet surface through three possible MECPs leading to the intermediates E, E1 and E2. From the intermediate E1 we observe the formation of the experimentally detected propyne and methylglyoxal, hereafter simply R4, whereas acetylene and the experimentally detected dimethylglyoxal, hereafter R5, are formed from the intermediate E2 through TS3. Propyne, together with the experimentally detected acetaldehyde and CO (hereafter: R3) is also formed from the intermediate E (2,5-dimethylfuran-3(2H)-one) through TS5, whereas from the same intermediate we also detected the formation of 3-penten-2-one and CO, hereafter R1, through TS1 and TS2. Differently from the intermediate C, for the initial adduct D we could locate a reaction route along the triplet surface (see the green line in the Figure 3) eventually leading to E5 through a C-O bond fission followed up with a McLafferty rearrangement-like H-shift from one methyl group to the opposite oxygen. This latter intermediate may then jump onto the singlet surface to form 3-buten-2-one and ketene, hereafter R6, by passing through TS7 or 1,2-diacetyl ethylene, hereafter R2, through TS6. This latter species can be also formed upon direct cross of the species D on the singlet surface. Note that, notwithstanding the apparent feasibility for adduct D to undergo the ISC falling

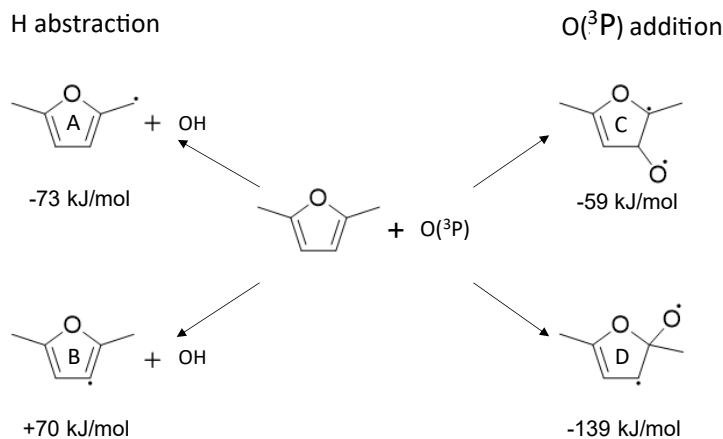


Fig. 2 Reaction energies for H abstraction and  $\text{O}(^3\text{P})$  addition calculated using the CBS-QB3 composite method.

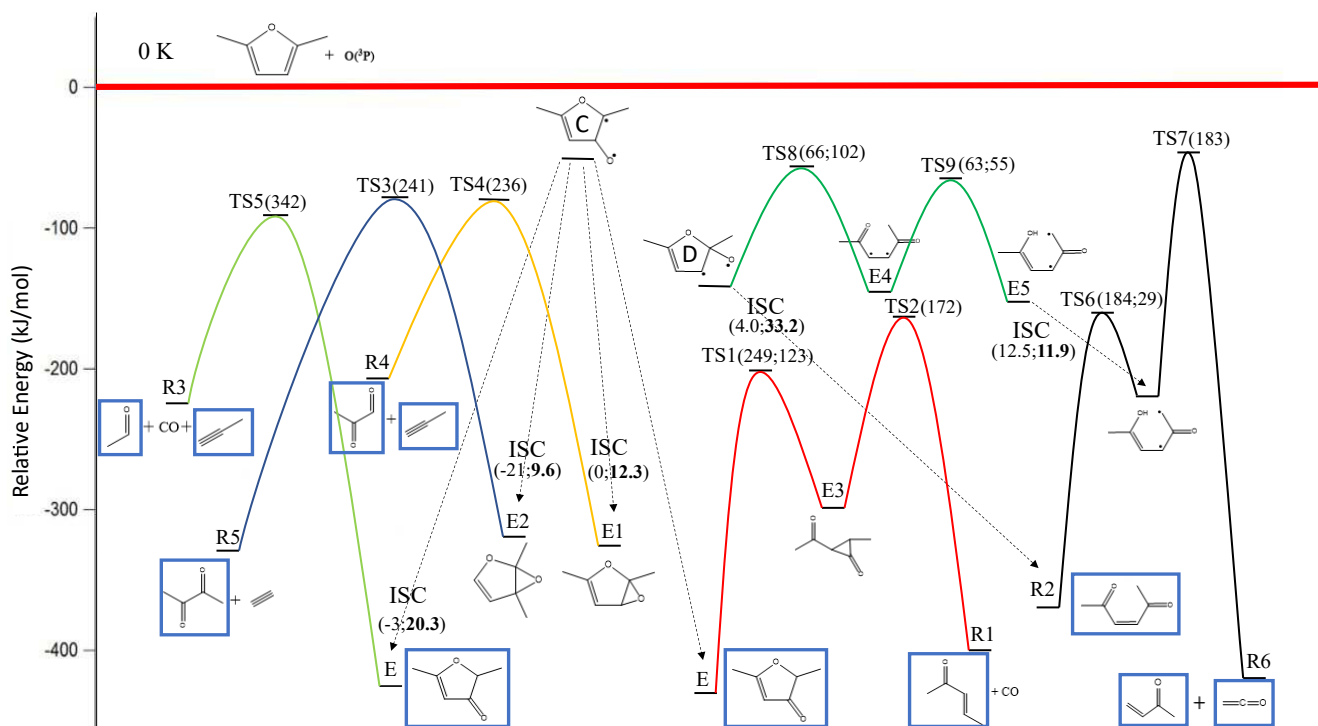
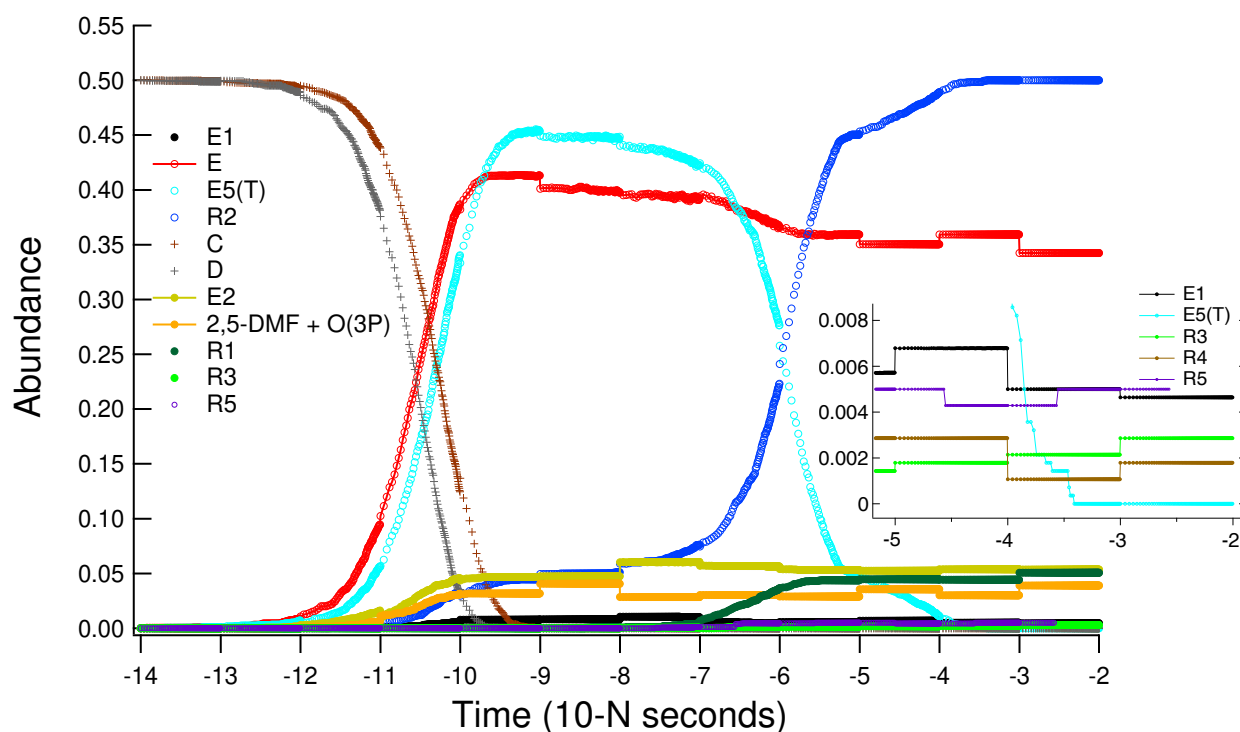


Fig. 3 Triplet and singlet potential energy surfaces of the adducts DMF-O. Dotted lines refer to the ISC connecting intermediates in the triplet and singlet surfaces with the spin-orbit coupling values ( $\text{cm}^{-1}$ ) indicated in bold along with the MECP barriers (kJ/mol) in the parentheses. The relative energies (kJ/mol) of transition states compared to the adjacent intermediates are indicated in the parentheses as well (reversible pathways are presented with either the forward and the reverse barriers). Identified products are highlighted with blue boxes. The red upper line indicates the thermochemical limit.



**Fig. 4** MultiWell kinetic modelling of the 2,5-DMF + O( $^3$ P) system in the  $10^{-16}$  –  $10^{-2}$  seconds time range including a close-up of the kinetics highlighting the  $10^{-5}$  –  $10^{-2}$  seconds time range. The observed discontinuities derive from numerical artifacts of the integration, not significantly affecting the final outcome, due to the use of different length of the simulations necessary for reporting the time-course of the different involved intermediates and products along the whole time range of interest.

into the E1 intermediate well, we did not manage to allocate any MECP connecting these two species on the triplet and singlet potential energy surface. Each of the above minima, TSs, and MECPs have been then used for outlining the kinetic model aimed at interpreting the products experimentally observed. The main difficulty, in this respect derives from the fact that, as shown in Figure 3, the reaction proceeds substantially without any tight barrier with respect to the reactants. This suggests that, under the experimental conditions of relatively high temperature and relatively low pressure, the thermalization channels, whose modeling is quite critical, are expected to be of great kinetic relevance and, hence, crucial for the final outcome. As a matter of fact, from the simulation of the whole reaction kinetics by assuming a complete thermalization, i.e., by means of canonical-TST, we could not observe the formation of any product. This finding, whose details can be found in the S.I., clearly indicates that in these conditions, as expected from the height of all the involved barriers, all the intermediates are completely stuck in the deep wells of the singlet surface without any chance to significantly evolve into the products in the millisecond timescale. Consequently, it is evident that, according to our model, most of the observed products should arise from a non-completely thermalized, i.e., relatively 'hot', fraction of the intermediates population even casting doubts on the full-validity of the statistical assumption on the basis of the RRKM theory.<sup>83</sup> Therefore, evading in the present study dynamical and non-statistical effects and following the procedure described in the Methods section, we carried out a 1-D Master Equation integration resembling the experimental conditions of

8 Torr and 550 K. The results are reported in Figure 4) and, for comparison, without bath gas (see S.I. for additional details), i.e., in the fully non-thermal conditions, for roughly estimating the fraction of non-thermalized population mainly responsible of the observed chemistry. By comparing the above kinetics at 8 Torr with the the zero-pressure limit and the high-pressure limit (see S.I. on these simulations), in particular considering the relative amount of the deep-well intermediates in the millisecond timescale, we have roughly evaluated a 10% of non-thermalized population accounting for the observed products in the conditions of the experiment. From Figure 4 we observe a very rapid formation of intermediate E, indicating a very efficient ISC from intermediate C, immediately followed by E2 and R2 arising from adducts C and D, respectively, within  $10^{-10}$  s. On the other hand, E5 and E1 formation, at about  $10^{-7}$  s, appear to be as slower processes with the latter also formed in rather low relative concentration. Such a delay may be ascribed, in the two cases, to different reasons. In fact, whereas the formation of E5(T) requires a certain number of intermediates, for E1 we might invoke slowing effects due to the the intrinsic features of the MECP, which contributes to the  $k(E)$  lowering. As a matter of fact, such a MECP, if compared to the other MECPs, is characterized not only by a lower SOC and a slightly higher barrier but also, as reported in the S.I., by a repertoire of high frequencies, which means that is a rather rigid structure with a reduced number of accessible states. Other aspects emerged by Figure 4 deserve additional remarks. First of all, we note that the back-dissociation channel of the initial adducts, in the present conditions, is far from being negligible. Moreover, the

kinetic model accounts for the formation of the long-lived intermediates E2, which is not detected in the experiment, due to the fact that the E2 cation has been found to be unbound, thus impossible to be observed in the MPIMS experiment. Finally, among the intermediates and the products described by the kinetic model, it is worthwhile to highlight the very fast formation of R2 and E and, although less efficiently, of R1 and E2. While R6 cannot be formed owing the gap between TS6 and TS7 energy barriers with respect to E5(S), the other products, including R3, R4, and R5 are formed with a relative concentration of roughly 0.5%, much lower than R1. Such a result might appear rather surprising as far as the height of the corresponding barriers are concerned. Hence it is clear that in these cases the ISCs must play a kinetically very relevant role. Therefore, given the severe approximations adopted for the non-adiabatic channels, we expect the final result to be quantitatively affected by a non-negligible level of uncertainty as shown in the next paragraph.

### 4.3 Branching Fractions

We calculated and compared the experimental and theoretical relative concentrations of the primary products with respect to the reactant, i.e., branching fractions (BF). Ion intensities of each detected signal are related to the concentrations of the species as described by the following equation:

$$S_i(E) = k\sigma_i(E)\delta_i C_i \quad (3)$$

where  $C_i$  is the concentration of the species,  $\sigma_i(E)$  is the photoionization cross-section of the species at the photon energy  $E$ ,  $k$  is the instrumental constant,  $S_i(E)$  is the ion signal at the specified photon energy integrated over a specific time range, and  $\delta_i$  is the mass discrimination factor accounting for the mass-dependent response of the instrument, here approximately equivalent to the mass of the species  $i$  raised to the power of 0.67.<sup>84</sup> By employing Equation 3, we calculated the BF as follows:

$$\frac{C_p}{C_r} = \frac{\frac{S_p}{\sigma_p \delta_p}}{\frac{S_r}{\sigma_r \delta_r}} = \frac{S_p \sigma_r \delta_r}{S_r \sigma_p \delta_p} = \frac{S_p \sigma_r}{S_r \sigma_p} \left( \frac{m_r}{m_p} \right)^{0.67} \quad (4)$$

where p and r stand for product and reactant, respectively. Because the photoionization cross-sections of 3-penten-2-one is not available in the literature, we estimated it by recording absolute photoionization spectrum and measuring a value of  $30.5 \pm 1.7$  Mb at 11 eV. Using the literature photoionization cross-section of 2,5-DMF and adding the estimated value of 13 Mb for the photoionization cross-section of the carbonyl group from Bobeldijk et al.<sup>85</sup> we obtained a value of  $43.2 \pm 12.9$  Mb for 2,5-dimethylfuran-3(2H)-one at 11 eV. For methylglyoxal and dimethylglyoxal cross-sections, we used the acetone and acetaldehyde photoionization cross-sections by Cool et al.<sup>73,74</sup> to obtain  $18 \pm 9$  and  $20 \pm 10$  Mb for methylglyoxal and dimethylglyoxal, respectively. Finally, we employed the same procedure with diacetyl ethylene by referencing it to the dimethylglyoxal cross-sections, to compute  $34 \pm 17$  Mb at 11 eV by adding the C=C and C-C group cross-sections from Bobeldijk et al.<sup>85</sup> We are aware that these are very rough estimations, thus affecting the

reliability of the experimental branching fractions, which are presented with a significant error. Concerning the theoretical values we have also re-evaluated the same quantities by modifying the barriers heights in order to improve the agreement with the experimental data.

The results are reported in Table 1. Theoretical BFs are in satisfactory agreement with the experimental values only for 1,2-diacetyl ethylene, propyne and acetaldehyde. A better match with the experimental values is obtained by lowering the TS2, TS3, TS4 and TS5 energy barriers of 10-15 kJ/mol. Such outcomes hence clearly indicate that the whole theoretical-computational picture cannot provide us with a fully quantitative answer. Whether such a limitation should be entirely ascribed to the small - but not negligible - errors of the CBS/DFT calculations or, rather, to the heavy approximations introduced for the kinetic model - e.g., lack of any dynamical effects or too crude approximations for the ISCs channels or deactivation channels - is beyond the actual purpose of this work, which is to provide an explanation of the identified primary products as deriving from non-thermal reactions and to unveil the significant role played by the ISC to account for the overall system dynamics.

## 5 Conclusions

Propyne, acetaldehyde, methylglyoxal, dimethylglyoxal, 3-penten-2-one, 2,5-dimethylfuran-3(2H)-one, and 1,2-diacetyl ethylene have been identified as the main primary products of  $O(^3P) + 2,5$ -dimethylfuran reaction in the gas phase at 8 Torr (He bath gas) and 550 K in the millisecond timescale. In order to rationalize such an experimental outcome, we carried out quantum chemical calculations and, on the basis of the located critical points as well as intersection between magnetic surfaces, we implemented a 1-D kinetic model. Notwithstanding the crude approximations introduced in the model, essentially related to (i) the use of a 1-D model, (ii) the collisional bimolecular quenching with the bath-gas, (iii) the kinetics of non-adiabatic channels and, finally, (iiii) the assumption of the fully-statistical behavior of the kinetics, we were able of reproducing all the observed products in the millisecond time range also suggesting that the whole chemistry observed in such a time scale should be entirely ascribed to the approximately 10% non-thermalized fraction of the intermediates population. A better agreement with the experimental data, prevented by the intrinsic errors coming from quantum-chemical calculations, could be reached by empirically modifying the heights of some of the involved barriers of 10-15 kJ/mol: a value close to the chemical accuracy expected from our calculations.<sup>51,52</sup> However, other errors deriving by the above reported possible sources of uncertainty should be better investigated with additional experiments, for instance using more sophisticated computational approaches or different bath gases to better address the quenching behavior and the relevant collisional deactivation parameters both for an experimental and a theoretical dynamics overview. Indeed, a gas with more degrees of freedom, such as  $N_2$  may favor the overall quenching process allowing the system to access the thermalization status in a faster and, therefore, more efficient way. Moreover, pressure-dependent experiments as low as 1 Torr or even lower if possible, would be

**Table 1** Experimental and computational (1-D model) branching fractions for reaction products: the experimental branching fractions are reported with the estimated relative error; the corrected branching fractions of the third column are calculated after reducing the TS2, TS3, TS4, and TS5 energy barriers of approximately 10-15 kJ/mol.

Branching Fraction	Experiment	Kinetic Model	Kinetic Model(corrected)
1,2-diacetyl ethylene	40.5 ± 21.3%	48%	48.5%
2,5-dimethylfuran-3(2H)-one	19.4 ± 6%	32.5%	24.5%
3-penten-2-one	26.4 ± 4.6%	5%	14.2%
propyne	1.7 ± 0.4%	0.5%	1.1%
acetaldehyde	1.9 ± 0.4%	0.3%	0.8%
methylglyoxal	2.9 ± 1.3%	0.2%	0.3%
dimethylglyoxal	9.5 ± 5%	0.5%	1.7%

notably useful to evaluate the efficiency of the thermalization process operated by the bath gas as a function of the pressure, and to accurately assess the non-thermalized/thermalized fraction of the intermediates population from an experimental point of view.

## Conflict of Interest

The authors declare no conflict of interest.

## Acknowledgments

This work is supported by the American Chemical Society – Petroleum Research Fund Grant 56067-UR6, the University of San Francisco via the Faculty Development Fund, and the U.S. Department of Energy Basic Energy Sciences under grant DE-FG02-87ER13792 (MIL). The authors express their gratitude to Drs Taatjes and Osborn from Sandia National Laboratories for the use of the experimental MPIMS apparatus. The Advanced Light Source is supported by the Director, Office of Science, Office of Basic Energy Sciences, of the U. S. Department of Energy under Contract No. DE-AC02-05CH11231.

## Notes and references

- M. Asif and T. Muneer, *Renewable and Sustainable Energy Reviews*, 2007, **11**, 1388–1413.
- S. Chu, Y. Cui and N. Liu, *Nature Materials*, 2016, **16**, 16–22.
- Y. Chisti, *Trends in Biotechnology*, 2008, **26**, 126–131.
- A. K. Agarwal, J. G. Gupta and A. Dhar, *Progress in Energy and Combustion Science*, 2017, **61**, 113–149.
- N. Yodsuwan, P. Kamonpatana, Y. Chisti and S. Sirisansaeneeyakul, *Journal of Biotechnology*, 2018, **267**, 71–78.
- S. U. K. Lawrence and S. K. S. P. Anantharaman, *International Journal of Current Microbiology and Applied Sciences*, 2017, **6**, 1259–1269.
- J. V. Gerpen, *Fuel Processing Technology*, 2005, **86**, 1097–1107.
- M. Eldeeb and B. Akih-Kumgeh, *Energies*, 2018, **11**, 512.
- R. Luque, L. Herrero-Davila, J. M. Campelo, J. H. Clark, J. M. Hidalgo, D. Luna, J. M. Marinas and A. A. Romero, *Energy & Environmental Science*, 2008, **1**, 542.
- J. B. Binder and R. T. Raines, *Journal of the American Chemical Society*, 2009, **131**, 1979–1985.
- S. Zhong, R. Daniel, H. Xu, J. Zhang, D. Turner, M. L. Wyszynski and P. Richards, *Energy & Fuels*, 2010, **24**, 2891–2899.
- Y. Qian, L. Zhu, Y. Wang and X. Lu, *Renewable and Sustainable Energy Reviews*, 2015, **41**, 633–646.
- H. Xu and C. Wang, *Biofuels from Lignocellulosic Biomass*, Wiley-VCH Verlag GmbH & Co. KGaA, 2016, pp. 105–129.
- Y. Román-Leshkov, C. J. Barrett, Z. Y. Liu and J. A. Dumesic, *Nature*, 2007, **447**, 982–985.
- L. Maat, H. van Bekkum, G. C. A. Luijkx, N. P. M. Huck and F. van Rantwijk, *HETEROCYCLES*, 2009, **77**, 1037.
- T. Thananathanachon and T. Rauchfuss, *Angewandte Chemie*, 2010, **122**, 6766–6768.
- M. Chidambaram and A. T. Bell, *Green Chemistry*, 2010, **12**, 1253.
- G. Tian, R. Daniel, H. Li, H. Xu, S. Shuai and P. Richards, *Energy & Fuels*, 2010, **24**, 3898–3905.
- Q. Zhang, G. Chen, Z. Zheng, H. Liu, J. Xu and M. Yao, *Fuel*, 2013, **103**, 730–735.
- Q. Zhang, M. Yao, J. Luo, H. Chen and X. Zhang, *Fuel*, 2013, **111**, 887–891.
- X. Liu, M. Yao, Y. Wang, Z. Wang, H. Jin and L. Wei, *Combustion and Flame*, 2015, **162**, 4586–4597.
- L. Wei, L. Tong, J. Xu, Z. Wang, H. Jin, M. Yao, Z. Zheng, H. Li and H. Xu, *Combustion Science and Technology*, 2014, **186**, 355–376.
- S. M. Aschmann, N. Nishino, J. Arey and R. Atkinson, *Environmental Science & Technology*, 2011, **45**, 1859–1865.
- E. Carrasco and G. Meloni, *The Journal of Physical Chemistry A*, 2018, **122**, 6118–6133.
- L.-S. Tran, Z. Wang, H.-H. Carstensen, C. Hemken, F. Battin-Leclerc and K. Kohse-Höinghaus, *Combustion and Flame*, 2017, **181**, 251–269.
- W. Leitner, J. Klankermayer, S. Pischinger, H. Pitsch and K. Kohse-Höinghaus, *Angewandte Chemie International Edition*, 2017, **56**, 5412–5452.
- L. S. Tran, B. Sirjean, P.-A. Glaude, R. Fournet and F. Battin-Leclerc, *Energy*, 2012, **43**, 4–18.
- M. A. Grela, V. T. Amorebieta and A. J. Colussi, *The Journal of Physical Chemistry*, 1985, **89**, 38–41.
- A. Lifshitz, C. Tamburu and R. Shashua, *The Journal of Physical Chemistry A*, 1998, **102**, 10655–10670.
- K. P. Somers, J. M. Simmie, F. Gillespie, C. Conroy, G. Black, W. K. Metcalfe, F. Battin-Leclerc, P. Dirrenberger, O. Herbinet, P.-A. Glaude, P. Dagaut, C. Togbé, K. Yasunaga, R. X. Fernandes, C. Lee, R. Tripathi and H. J. Curran, *Combustion and Flame*, 2013, **160**, 2291–2318.
- J. M. Simmie and W. K. Metcalfe, *The Journal of Physical Chemistry A*, 2011, **115**, 8877–8888.

- 32 B. Sirjean and R. Fournet, *Phys. Chem. Chem. Phys.*, 2013, **15**, 596–611.
- 33 H. Yoshizawa, H. Nagashima, Y. Murakami and K. Takahashi, *Chemistry Letters*, 2017, **46**, 1207–1210.
- 34 N. Balucani, F. Leonori and P. Casavecchia, *Energy*, 2012, **43**, 47–54.
- 35 F. Leonori, N. Balucani, V. Nevrlý, A. Bergeat, S. Falcinelli, G. Vanuzzo, P. Casavecchia and C. Cavallotti, *The Journal of Physical Chemistry C*, 2015, **119**, 14632–14652.
- 36 J. D. Savee, S. Borkar, O. Welz, B. Sztáray, C. A. Taatjes and D. L. Osborn, *The Journal of Physical Chemistry A*, 2015, **119**, 7388–7403.
- 37 T. L. Nguyen, L. Vereecken, X. J. Hou, M. T. Nguyen and J. Peeters, *The Journal of Physical Chemistry A*, 2005, **109**, 7489–7499.
- 38 C. Cavallotti, C. D. Falco, L. P. Maffei, A. Caracciolo, G. Vanuzzo, N. Balucani and P. Casavecchia, *The Journal of Physical Chemistry Letters*, 2020, **11**, 9621–9628.
- 39 J. A. Miller, R. J. Kee and C. K. Westbrook, *Annual Review of Physical Chemistry*, 1990, **41**, 345–387.
- 40 R. A. Marcus, W. L. Hase and K. Swamy, *The Journal of Physical Chemistry*, 1984, **88**, 6717–6720.
- 41 O. K. Rice and H. C. Ramsperger, *Journal of the American Chemical Society*, 1927, **49**, 1617–1629.
- 42 J. C. Lorquet and B. Leyh-Nihant, *The Journal of Physical Chemistry*, 1988, **92**, 4778–4783.
- 43 J. N. Harvey and M. Aschi, *Physical Chemistry Chemical Physics*, 1999, **1**, 5555–5563.
- 44 P. A. Heimann, M. Koike, C. W. Hsu, D. Blank, X. M. Yang, A. G. Suits, Y. T. Lee, M. Evans, C. Y. Ng, C. Flaim and H. A. Padmore, *Review of Scientific Instruments*, 1997, **68**, 1945–1951.
- 45 M. Y. Ng, J. Nelson, C. A. Taatjes, D. L. Osborn and G. Meloni, *The Journal of Physical Chemistry A*, 2014, **118**, 3735–3748.
- 46 A. W. Ray, C. A. Taatjes, O. Welz, D. L. Osborn and G. Meloni, *The Journal of Physical Chemistry A*, 2012, **116**, 6720–6730.
- 47 M. Y. Ng, B. M. Bryan, J. Nelson and G. Meloni, *The Journal of Physical Chemistry A*, 2015, **119**, 8667–8682.
- 48 D. L. Osborn, P. Zou, H. Johnsen, C. C. Hayden, C. A. Taatjes, V. D. Knyazev, S. W. North, D. S. Peterka, M. Ahmed and S. R. Leone, *Review of Scientific Instruments*, 2008, **79**, 104103.
- 49 J. Troe, *Zeitschrift für Physikalische Chemie*, 2000, **214**, 573–581.
- 50 A. Vandaele, C. Hermans, P. Simon, M. Carleer, R. Colin, S. Fally, M. Mérienne, A. Jenouvrier and B. Coquart, *Journal of Quantitative Spectroscopy and Radiative Transfer*, 1998, **59**, 171–184.
- 51 J. A. Montgomery, M. J. Frisch, J. W. Ochterski and G. A. Petersson, *The Journal of Chemical Physics*, 1999, **110**, 2822–2827.
- 52 J. A. Montgomery, M. J. Frisch, J. W. Ochterski and G. A. Petersson, *The Journal of Chemical Physics*, 2000, **112**, 6532–6542.
- 53 J.-D. Chai and M. Head-Gordon, *Physical Chemistry Chemical Physics*, 2008, **10**, 6615.
- 54 M. J. Frisch, G. W. Trucks, H. B. Schlegel, G. E. Scuseria, M. A. Robb, J. R. Cheeseman, G. Scalmani, V. Barone, B. Mennucci, G. A. Petersson, H. Nakatsuji, M. Caricato, X. Li, H. P. Hratchian, A. F. Izmaylov, J. Bloino, G. Zheng, J. L. Sonnenberg, M. Hada, M. Ehara, K. Toyota, R. Fukuda, J. Hasegawa, M. Ishida, T. Nakajima, Y. Honda, O. Kitao, H. Nakai, T. Vreven, J. A. Montgomery Jr, J. E. Peralta, F. Ogliaro, M. Bearpark, J. J. Heyd, E. Brothers, K. N. Kudin, V. N. Strohlov, R. Kobayashi, J. Normand, K. Raghavachari, A. Rendell, J. C. Burant, S. S. Iyengar, J. Tomasi, M. Cossi, N. Rega, J. M. Millam, M. Klene, J. E. Knox, J. B. Cross, V. Bakken, C. Adamo, J. Jaramillo, R. Gomperts, R. E. Stratmann, O. Yazyev, A. J. Austin, R. Cammi, C. Pomelli, J. W. Ochterski, R. L. Martin, K. Morokuma, V. G. Zakrzewski, G. A. Voth, P. Salvador, J. J. Dannenberg, S. Dapprich, A. D. Daniels, O. Farkas, J. B. Foresman, J. V. Ortiz, J. Cioslowski and D. J. Fox, *Gaussian 09., revision A.02.*, 2016, Gaussian, Inc.: Wallingford, CT.
- 55 D. L. Baulch, C. T. Bowman, C. J. Cobos, R. A. Cox, T. Just, J. A. Kerr, M. J. Pilling, D. Stocker, J. Troe, W. Tsang, R. W. Walker and J. Warnatz, *Journal of Physical and Chemical Reference Data*, 2005, **34**, 757–1397.
- 56 T. A. Cool, A. McIlroy, F. Qi, P. R. Westmoreland, L. Poisson, D. S. Peterka and M. Ahmed, *Review of Scientific Instruments*, 2005, **76**, 094102.
- 57 M. A. Oehlschlaeger, D. F. Davidson and R. K. Hanson, *The Journal of Physical Chemistry A*, 2006, **110**, 9867–9873.
- 58 F. Santoro, A. Lami, R. Improta and V. Barone, *The Journal of Chemical Physics*, 2007, **126**, 184102.
- 59 K. Fukui, *The Journal of Physical Chemistry*, 1970, **74**, 4161–4163.
- 60 K. Fukui, *Accounts of Chemical Research*, 1981, **14**, 363–368.
- 61 J. N. Harvey, *Phys. Chem. Chem. Phys.*, 2007, **9**, 331–343.
- 62 J. N. Harvey, M. Aschi, H. Schwarz and W. Koch, *Theoretical Chemistry Accounts: Theory, Computation, and Modeling (Theoretica Chimica Acta)*, 1998, **99**, 95–99.
- 63 N. Koga and K. Morokuma, *Chemical Physics Letters*, 1985, **119**, 371–374.
- 64 G. M. J. Barca, C. Bertonni, L. Carrington, D. Datta, N. De Silva, J. E. Deustua, D. G. Fedorov, J. R. Gour, A. O. Gunina, E. Guidez, T. Harville, S. Irlé, J. Ivanic, K. Kowalski, S. S. Leang, H. Li, W. Li, J. J. Lutz, I. Magoulas, J. Mato, V. Mironov, H. Nakata, B. Q. Pham, P. Piecuch, D. Poole, S. R. Pruitt, A. P. Rendell, L. B. Roskop, K. Ruedenberg, T. Sattasathuchana, M. W. Schmidt, J. Shen, L. Slipchenko, M. Sosonkina, V. Sundriyal, A. Tiwari, J. L. Galvez Vallejo, B. Westheimer, M. Wloch, P. Xu, F. Zahariev and M. S. Gordon, *The Journal of Chemical Physics*, 2020, **152**, 154102.
- 65 J. R. Barker, T. L. Nguyen, J. F. Stanton, C. Aieta, M. Ceotto, F. Gabas, T. J. D. Kumar, C. G. L. Li, L. L. Lohr, A. Maranzana, N. F. Ortiz, J. M. Preses, J. M. Simmie, J. A. Sonk, and P. J. Stimac, *MultiWell-2019 Software Suite*, 2019, J. R. Barker, University of Michigan, Ann Arbor, Michigan, USA; <http://clasp-research.engin.umich.edu/multiwell/>.

- 66 J. R. Barker, *International Journal of Chemical Kinetics*, 2009, **41**, 748–763.
- 67 C. Eckart, *Physical Review*, 1930, **35**, 1303–1309.
- 68 T. L. Nguyen, B. C. Xue, R. E. Weston, J. R. Barker and J. F. Stanton, *The Journal of Physical Chemistry Letters*, 2012, **3**, 1549–1553.
- 69 R. E. Weston, T. L. Nguyen, J. F. Stanton and J. R. Barker, *The Journal of Physical Chemistry A*, 2013, **117**, 821–835.
- 70 H. Hippler, J. Troe and H. J. Wendelken, *The Journal of Chemical Physics*, 1983, **78**, 6709–6717.
- 71 B. Yang, L. Gagliardi and D. G. Truhlar, *Physical Chemistry Chemical Physics*, 2018, **20**, 4129–4136.
- 72 K. Aidas, C. Angeli, K. L. Bak, V. Bakken, R. Bast, L. Boman, O. Christiansen, R. Cimraglia, S. Coriani, P. Dahle, E. K. Dal-skov, U. Ekström, T. Enevoldsen, J. J. Eriksen, P. Ettenhuber, B. Fernández, L. Ferrighi, H. Fliegl, L. Frediani, K. Hald, A. Halkier, C. Hättig, H. Heiberg, T. Helgaker, A. C. Hen-num, H. Hettrema, E. Hjertenæs, S. Høst, I.-M. Høyvik, M. F. Iozzi, B. Jansík, H. J. Aa. Jensen, D. Jonsson, P. Jørgensen, J. Kauczor, S. Kirpekar, T. Kjærgaard, W. Klopper, S. Knecht, R. Kobayashi, H. Koch, J. Kongsted, A. Krapp, K. Kristensen, A. Ligabue, O. B. Lutnæs, J. I. Melo, K. V. Mikkelsen, R. H. Myhre, C. Neiss, C. B. Nielsen, P. Norman, J. Olsen, J. M. H. Olsen, A. Osted, M. J. Packer, F. Pawłowski, T. B. Pedersen, P. F. Provasi, S. Reine, Z. Rinkevicius, T. A. Ruden, K. Ruud, V. V. Rybkin, P. Sałek, C. C. M. Samson, A. S. de Merás, T. Saue, S. P. A. Sauer, B. Schimmelpfennig, K. Sneskov, A. H. Steindal, K. O. Sylvester-Hvid, P. R. Taylor, A. M. Teale, E. I. Tellgren, D. P. Tew, A. J. Thorvaldsen, L. Thøgersen, O. Vahtras, M. A. Watson, D. J. D. Wilson, M. Ziolkowski and H. Ågren, *WIREs Comput. Mol. Sci.*, 2014, **4**, 269–284.
- 73 T. A. Cool, J. Wang, K. Nakajima, C. A. Taatjes and A. Mcllroy, *International Journal of Mass Spectrometry*, 2005, **247**, 18–27.
- 74 T. A. Cool, K. Nakajima, T. A. Mostefaoui, F. Qi, A. Mcllroy, P. R. Westmoreland, M. E. Law, L. Poisson, D. S. Peterka and M. Ahmed, *The Journal of Chemical Physics*, 2003, **119**, 8356–8365.
- 75 B. Yang, J. Wang, T. A. Cool, N. Hansen, S. Skeen and D. L. Osborn, *International Journal of Mass Spectrometry*, 2012, **309**, 118–128.
- 76 C. A. Taatjes, *Science*, 2005, **308**, 1887–1889.
- 77 A. M. Scheer, A. J. Eskola, D. L. Osborn, L. Sheps and C. A. Taatjes, *The Journal of Physical Chemistry A*, 2016, **120**, 8625–8636.
- 78 W. von Niessen, G. Bieri and L. Åsbrink, *Journal of Electron Spectroscopy and Related Phenomena*, 1980, **21**, 175–191.
- 79 E. Carrasco, K. J. Smith and G. Meloni, *The Journal of Physical Chemistry A*, 2017, **122**, 280–291.
- 80 R. J. Cvetanović, *Journal of Physical and Chemical Reference Data*, 1987, **16**, 261–326.
- 81 R. J. Cvetanovic and D. L. Singleton, *Reviews of Chemical Intermediates*, 1984, **5**, 183–226.
- 82 R. J. Cvetanović, *Advances in Photochemistry*, John Wiley & Sons, Inc., 2007, pp. 115–182.
- 83 B. Jayee and W. L. Hase, *Annual Review of Physical Chemistry*, 2020, **71**, 289–313.
- 84 O. Welz, J. Zádor, J. D. Savee, M. Y. Ng, G. Meloni, R. X. Fernandes, L. Sheps, B. A. Simmons, T. S. Lee, D. L. Osborn and C. A. Taatjes, *Physical Chemistry Chemical Physics*, 2012, **14**, 3112.
- 85 M. Bobeldijk, W. van der Zande and P. Kistemaker, *Chemical Physics*, 1994, **179**, 125–130.